13

ETMM

ETMM13 Rhodes, Greece
15-17 September, 2021.

CONFERENCE PROCEEDINGS

LES OF JET FLOWS ISSUING FROM LONG, CONTRACTED AND ORIFICE TYPE TRIANGULAR NOZZLES AT VARIOUS ASPECT RATIOS

***J. Stempka*[1,*], *A. Tyliszczak*[1], *A. Boguslawski*[1] *and B. Geurts*[2]**

[1] ***Czestochowa University of Technology,***
Faculty of Mechanical Engineering and Computer Science,
Department of Thermal Machinery, Armii Krajowej 21, 42-201 Czestochowa, Poland
[2] ***University of Twente, P.O. Box 217, 7500 AE Enschede, The Netherlands***

[*]**stempka@imc.pcz.pl**

Abstract

In the current study we perform LES of the jets issuing from the triangular nozzles with various aspect ratios (ARs) and various end sections, i.e., smooth transition, straight pipe, short contracting and orifice plate. It is shown that increasing the AR of a nozzle speeds-up the decay of the axial velocity and increases the growth of its fluctuations in the near-field. However, the impact of the AR on the jet behaviour strongly depends on the type of the exit nozzle section.

1 Introduction

Passive control of the jet flows is most often realised by shaping the nozzles. It is regarded as the simplest way allowing to obtain practically desired jet characteristics, e.g., enhanced mixing rates and entrainment. Even though such geometrical modifications can be applied easily, the actual outcome is difficult to predict by intuition. For instance, it turns out that the jets issuing from sharp-edged orifices are more energetic compared to the jets generated by smoothly contoured nozzles (Mi and Nathan 2010; Azad et al. 2012), whereas the jets issuing from asymmetric or polygonal nozzles feature in emergence of flow structures that enhance the mixing intensity (Gutmark and Grinstein, 1999; Quinn, 2005). In the experimental study of Mi and Nathan (2010) put an effort into recognition of the impact of smoothly contracting and orifice-type (OP) nozzles on the jet dynamics. This work was devoted to triangular nozzles (equilateral and isosceles triangular with various aspect ratios (AR)), among others, which in previous research showed remarkably different behaviour compared to the other nozzle shapes, e.g., circular or square. Among all analysed configurations the results obtained using the isosceles-triangular nozzle of $AR = 2.5$, characterised by the fastest velocity decay rate in the near-field, enhanced mixing and the largest spreading rate. The triangular nozzles show tendency to shorten the potential core of the jet and intensify turbulence level was recently showed experimentally by Aleyasin et al. (2018) for a sharp contraction nozzle in a wide range of the Reynolds number ($Re = 6000$-$20\,000$). It was shown by the author that the potential core length was about 16%–30% shorter in the triangular jets compared to the round jets, implying enhanced mixing performance in the near-field region of the triangular jets. Additionally, the authors showed that in case of round jet increasing Re above 6000 reduces the mixing performance in contrast to the triangular jets in which the mixing characteristics were almost independent of Re. One of the indicators was the swirling strength which revealed faster turbulent diffusion from the shear layers toward the centreline in the triangular jets comparing to the round jets. The impact of the nozzle exit shape was studied experimentally by Quinn et al. (2013). The configurations under investigations were: triangular isosceles OP nozzles of $AR \approx 1.9$ and $AR \approx 0.09$ and were compared to the two circular ones: OP and contoured nozzle. For $Re = 168\,000$ the authors showed a higher streamwise centreline velocity decay in low AR jet. The potential core length was the shortest for OP nozzle and $AR \approx 0.09$, on the other hand it was the longest for the contoured nozzle circular jet. The axis-switching phenomena was discerned for the high AR nozzle but no evidence of such was reported for the low AR jet.

The current studies extend on the jets issuing from the triangular nozzles with various ARs and various end sections. It is unknown whether the exceptional characteristics of the jet studied by Mi and Nathan (2010) ($AR = 2.5$, orifice-type nozzle) is preserved if the nozzle is a long pipe or if it ends by a sharp contraction. In the present research we focused on this issue and assessed the effect of the jet nozzle aspect ratio, i.e., $AR = 1.0, 1.5, 2.0, 2.5, 3.0$ and the nozzle type, i.e., a straight pipe (SP), short contraction (SC) and orifice plate. The research is performed applying Large Eddy Simulation (LES) and an in-house high-order solver SAILOR (Tyliszczak, 2014). The results obtained allowed us to show that depending on

the nozzle type the jets at various AR behave significantly different.

2 Configuration

Similarly as in the experimental study of Mi and Nathan (2010) we consider the jets characterized by $Re = U_b D_e/\nu = 15\,000$, defined based on the bulk jet velocity U_b, equivalent nozzle diameter D_e, which is kept constant for all analysed nozzle configurations and air kinematic viscosity ν. The Re value was intentionally chosen since as shown by Aleyasin et al. (2018) the triangular jets at $Re = 15\,000$ generally feature in similar characteristics as the higher Re numbers cases and the mixing efficiency seems not be too much affected.

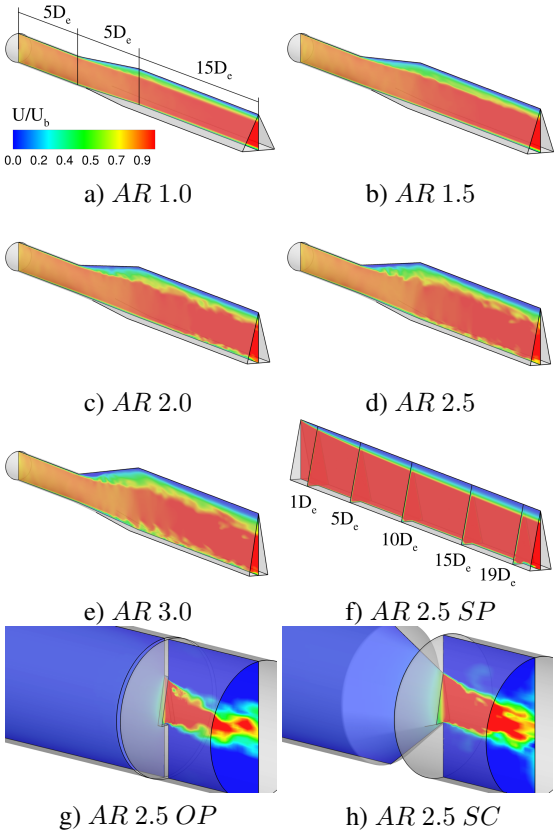

Figure 1: Schematic views of the analysed nozzles types.

The computations were performed in two stages. In the first one, we applied the ANSYS Fluent solver to model the flow inside the nozzles and acquired the velocity signals (of a duration $300 D_e/U_b$), which were then used as the inlet boundary conditions for the second part of the simulations. The main computations were carried out using the SAILOR code. In that stage we modelled the flow in a rectangular domain of dimensions $8D_e \times 8D_e \times 28D_e$. The geometries used to generate the inlet velocity signals are presented in Fig. 1. The subfigures (a)-(e) show the geometries of the smooth transition nozzles with initial circular cross-section changing into the triangular one. Subfigure (f) depicts the SP nozzle geometry with the cross-sections indicating the locations of the inlet signal acquisition, while the subfigures (g) and (h) show the geometries of the OP and SC nozzles.

Referring to a particular case throughout the text we use abbreviations containing: AR (aspect ratio) followed by the value of AR, i.e, 1.0, 1.5, 2.0, 2.5 or 3.0. The abbreviation ends with the symbol denoting the nozzle type, i.e., OP, SC or SP (smooth transition is left without any symbol). In case of SP isosceles triangular nozzle, one of the values 1, 5, 10, 15 or 19 used in the symbol indicates the location expressed in y/D_e units, where the inlet signal was a gathered.

Modelling

In this paper we consider incompressible flow modelled through the incompressible LES filtered Navier-Stokes equations which can be found in many textbooks, i.e., Geurts (2021). The main numerical simulations were carried out using an in-house LES high-order compact difference code developed and verified by Tyliszczak (2014). The SAILOR code is based on the projection method for the pressure-velocity coupling with time integration performed by a predictor-corrector (Adams-Bashforth/Adams-Moulton) method. The spatial discretization is based on the compact difference method up to 10^{th} order on half-staggered meshes. For sub-grid stresses modelling it exploits the Vreman model. As already mentioned, for generating the inlet velocity signals we used ANSYS Fluent software with LES turbulence model, applying the WALE sub-grid scales model.

3 Results

Figure 2 presents the centreline profiles of the normalized time-averaged axial velocity U_c/U_m (U_m denoting the maximum velocity value) (a), its inverse (b), RMS of the axial velocity fluctuations (U_{RMS}) (c), and its normalized values U_{RMS}/U_c (d), for all the analysed cases. It can be seen in Fig. 2a) and b) that with the increasing nozzle AR the velocity profiles exhibit the expected trend of a faster velocity decay. The results for AR 1.0 and AR 2.5 up to the intermediate-field are in good agreement with the experimental data of Mi and Nathan (2010) (note that experiments were performed using OP nozzle). For OP nozzle we obtained a good agreement in the near-field however underestimation is evident in the intermediate-field. On the other hand, the results from SP isosceles traingular nozzle show a distinct behaviour. The results in Fig. 2a) indicate that U_c/U_m profiles almost overlap in the near to intermediate field, differently from the smooth transition cases. However, from Fig. 2b) one can read that the velocity decay rate increases in the far-field while progressing the plane of the inlet signal acquisition towards the nozzle exit.

The velocity fluctuations grow downstream the jet

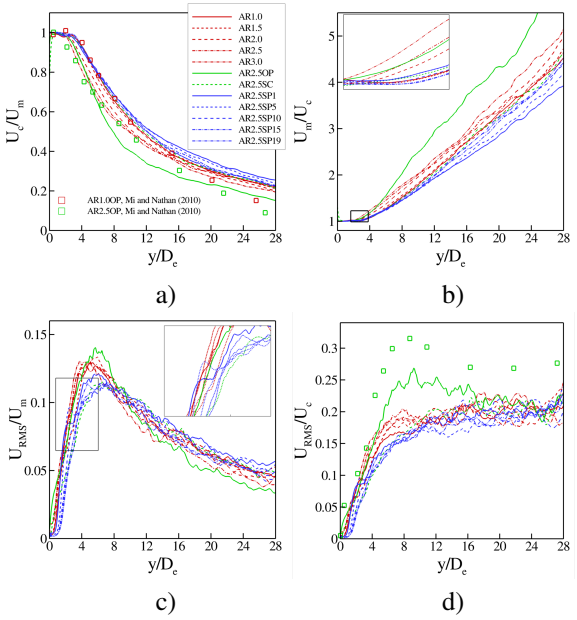

Figure 2: Centreline profiles of the time-averaged U_c normalized by U_m (a), its inverse (b), RMS of the axial velocity fluctuations U_{RMS} (c), and its normalized values U_{RMS}/U_c (d).

as the turbulent structures evolve in the shear layer. The centreline U_{RMS} and U_{RMS}/U_c profiles in general indicate that the velocity fluctuations in SP jets of $AR = 2.5$ are weaker than in the other. From Fig. 2c) a faster rate of U_{RMS} growth for smooth transition nozzles compared to SP can be found. Also, by increasing AR the peak value of U_{RMS} grows. Faster increase of U_{RMS} can be attributed to the quicker growth of the turbulent structures towards the centreline. This indicates the enhancement in near-filed mixing rate attributed to smooth transition nozzles with a high AR. In Fig. 2d) we indicated the experimental results of Mi and Nathan (2010). Even though the underestimation is evident we were able to well capture the trend of the characteristic broad peak in U_{RMS}/U_c as well as its axial location. The origin of that peak is discussed in the following sections. One can note the characteristics non-growing regions of U_{RMS} in the zoom in Fig. 2c) for SP nozzle. These are due to the merging of multiple shear layers stemming from the non-circular nozzle geometry as noted by Quinn et al. (2013).

The profiles of U_m/U_c apparently asymptote to a linear decay. Therefore for getting a further insight into the velocity characteristics we calculated the parameters of the linear fits of the results from Fig. 2b) for $y/D_e > 10$, following the expression:

$$\frac{U_m}{U_c} = K_u \left(\frac{y - y_0}{D_e} \right), \qquad (1)$$

where y_0/D_e is called the jet virtual origin and K_u is velocity decaying rate. Additionally, we estimated the potential core lengths L_c/D_e based on the value $0.98U_m$. These results can be found in Tab. 1.

Table 1: Table presenting the values from fitting the axial velocity profiles to Eq. (1) and L_c values.

Case	$\frac{y_0}{D_e}$	K_u	$\frac{L_c}{D_e}$	Re
$AR\,1.0$	-0.21	0.156	3.3	15 000
$AR\,1.5$	-0.25	0.153	3.3	15 000
$AR\,2.0$	-0.31	0.159	2.7	15 000
$AR\,2.5$	-0.57	0.140	2.4	15 000
$AR\,3.0$	-0.04	0.188	2.2	15 000
$AR\,2.5\,OP$	-0.24	0.210	2.1	15 000
$AR\,2.5\,OP$ [b)]	—	0.203	—	15 000
$AR\,1.0\,OP$ [c)]	—	0.196	—	184 000
$AR\,2.5\,SC$	-0.17	0.158	2.8	15 000
$AR\,1.0\,SC$ [a)]	—	0.156	—	13 800
$AR\,1.0\,SC$ [a)]	—	0.157	—	20 000
$AR\,2.5\,SP1$	-0.30	0.134	3.1	15 000
$AR\,2.5\,SP5$	-0.19	0.141	3.1	15 000
$AR\,2.5\,SP10$	-0.37	0.138	3.3	15 000
$AR\,2.5\,SP15$	-0.11	0.154	3.3	15 000
$AR\,2.5\,SP19$	-0.29	0.148	3.3	15 000

[a)] Aleyasin et al. (2018) [b)] Mi and Nathan (2010)
[c)] Quinn (2005)

The estimated K_u values confirm that the jets issuing from SP nozzle characterize slower velocity decay than the ones originating from smooth transition nozzle. For SC and OP nozzles K_u values agree well with the literature data. The velocity decay rate in OP jet is the fastest while L_c/D_e is the shortest one. It should be noted that L_c is often regarded as an indicator of the mixing efficiency in the near-field region. On the other hand K_u parameter measures the mixing performance for the intermediate region. Both these parameters for the OP case have the highest values. As can be seen in Tab. 1 the velocity in SC case starts to decay 25% farther than in OP and this aligns well with the experimental observations of Aleyasin et al. (2018). Similarly as in experiment of Mi and Nathan (2010) we reported a shorter L_c for the isosceles traingular jets compared to the equilateral one.

Inlet profiles characteristics

Figure 3 shows U/U_c exit profiles (left column) and turbulence intensity ($Ti = U/U_b$) (right column) from the axial distance $y/D_e = 0.1$ for the cases: smooth transition nozzles (a), OP, SC nozzles (b) and SP nozzle (c), along major (r_1) and minor (r_2) axes. The profiles exhibit substantially different behaviours leading to the distinct properties of the issuing jets. For cases shown in Fig. 3a) one may observe the profiles change its horizontal extends due to nozzle AR in a predictable way. However, with increasing the jet AR the velocity profiles clearly deviate from the top hat shape. This, together with increasing values of Ti, along the nozzle base and towards its corner suggests a stronger turbulent transport toward the axis accompanied by the momentum retardation in the vicinity

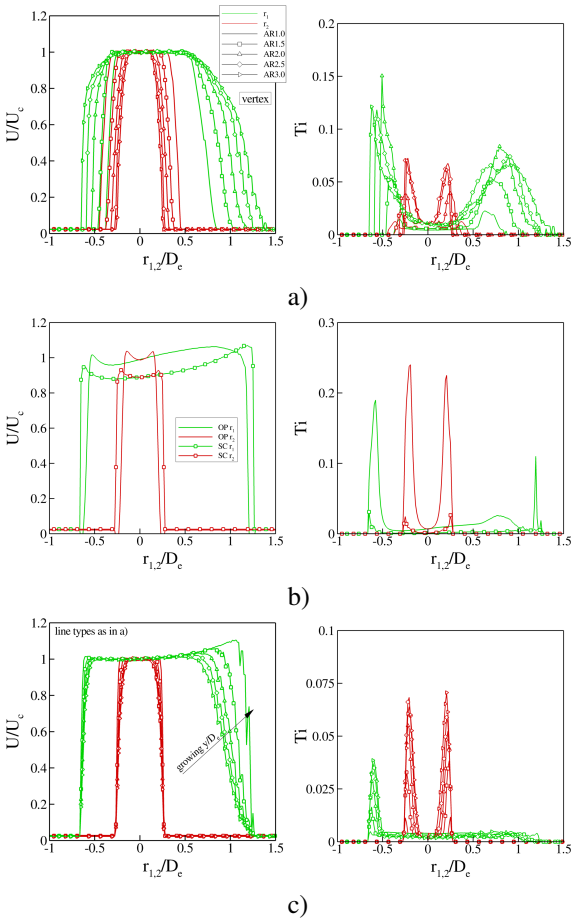

Figure 3: Nozzle exits U/U_c (left column) and Ti (right column) profiles at $y/D_e = 0.1$ for cases: a) smooth transition, b) OP and SC. Profiles in c) correspond to the consecutive planes along SP case. Profiles denoted as r_1 and r_2 extracted along the major and minor axes, respectively.

of the walls. This has direct impact on the development of the issuing shear layer. The velocity profiles of OP and SC jets shown in Fig. 3b) are significantly steeper near the nozzle walls, along direction r_1. This results from very short passage before exiting the nozzle, insufficient for the boundary layer development. Therefore, the velocity profiles are more alike on both sides. They present characteristic local minima situated in the vicinity of the axis. Accompanying Ti profiles present also very distinct features. In particular Ti peaks for OP case have values higher than in other cases.

The velocity profiles of SP cases exhibit typical channel like development except for a strong deviation is seen in the corner vicinity. The corner acts as turbulence suppression as no peak in Ti is found in that region. This feature makes the profiles distinct from the smooth transition cases where the peaks are present. Therefore, it can be concluded that cross-sectional change leads to the boundary layer turbularization in the corner vicinity in contrary to what is observed in the long straight channel. Comparing the velocity profiles in smooth transition case to the SP we can conclude that the retardation of the momentum in the corner vicinity is not caused by the turbulent diffusion but rather by the viscous shear. This contrasts with the smooth transition cases in which the retardation was attributed to the former process.

In the Tab. 2 the estimates of the parameters characterizing the inlet profiles are given. In particular, the momentum thicknesses in a vicinity of the nozzle regions, i.e., sides (s), base (b), corner (c) and the respective shape factors (H).

Table 2: Table presenting the characteristic parameters of the inlet velocity profiles.

Case	$\frac{D_e}{\theta_s}$	$\frac{D_e}{\theta_b}$	$\frac{D_e}{\theta_c}$	H_s	H_b	H_c
AR 1.0	15.1	16.3	6.8	2.2	2.0	2.5
AR 1.5	16.0	15.5	4.8	2.2	2.2	2.4
AR 2.0	15.1	11.5	4.0	2.4	1.6	2.5
AR 2.5	16.1	9.4	3.2	2.1	1.3	2.4
AR 3.0	16.7	8.4	2.9	2.4	1.3	2.5
AR 2.5 OP	35.1	29.0	26.5	2.8	2.4	3.3
AR 2.5 SC	57.6	193.0	232.8	3.0	1.0	1.3
AR 2.5 $SP1$	44.8	42.9	14.3	3.3	1.6	2.5
AR 2.5 $SP5$	26.2	25.4	7.0	2.8	2.0	3.2
AR 2.5 $SP10$	22.0	20.4	5.4	1.8	2.0	3.0
AR 2.5 $SP15$	19.2	17.9	4.5	1.9	2.0	3.1
AR 2.5 $SP19$	17.5	16.4	4.2	1.6	2.0	3.1

Overall, θ_s, θ_b and H_s, H_b values are more uniform in case of SP nozzle for AR 2.5 than in smooth transition nozzle. This is because the geometrical hump accelerates a boundary layer development. In all the cases other than SC, θ_c (H_c) have the lowest (highest) values. This is a consequence of the momentum retardation in the corner region. Most notable differences are found for SC and OP nozzles. The OP nozzle introduces the most uniform θ along the perimeter. On the other extreme the SC nozzle makes the issuing boundary layer the thinnest one. This alters the size of turbulent structures originating from the emerging shear layer.

Averaged velocity distributions

The impact of nozzle shape on jets structure in the near-fields is qualitatively shown in Fig. 4. The images present U/U_b distributions drawn on the planes aligned with the major nozzle axis r_1. Most pronounced differences in shape and L_c are evidenced. Clearly, the nozzle geometry impacts the shear layer thickness and the rate of its growth.

In Fig. 5 the contours of the averaged axial velocity are shown on the planes perpendicular to the jet axis of the cases, i.e., (a) AR 1.0, (b) AR 2.0, (c) AR 2.5 OP and (d) AR 2.5 OP. They present interesting and distinct features representative also for other cases. Case (a) shows evolution of the velocity iso-contours typical for low AR nozzles (1.0 and 1.5).

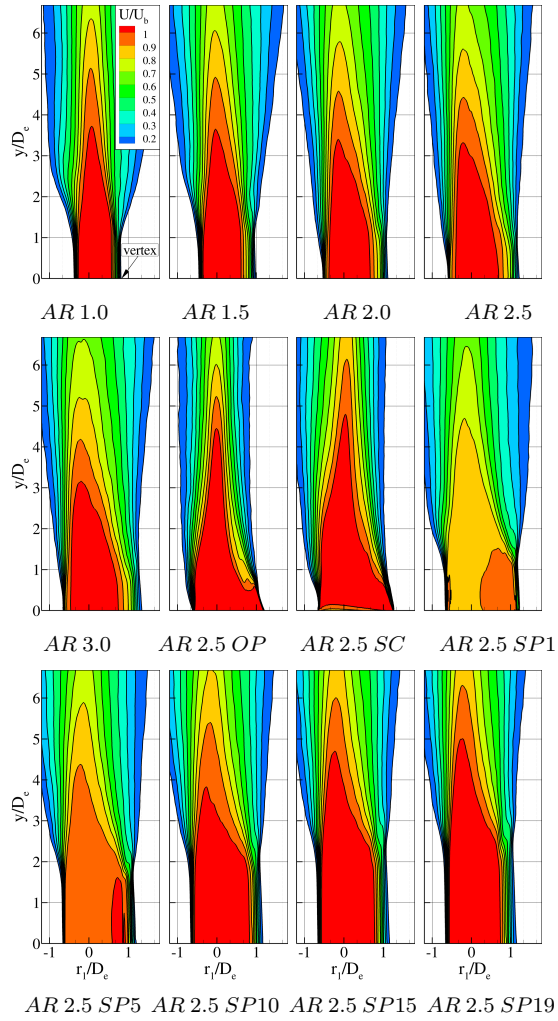

Figure 4: Normalized axial velocity distributions drawn on the planes aligned with the major nozzle axis.

Contours evolve downstream with growing waviness of the outer iso-lines in the directions of extreme positive/negative curvature, indicated by the arrows. The curvature is attributed to the alternate inward and outward mass fluxes. The waviness is not present for the smooth transition nozzles with $AR > 2.0$ and in SP nozzle. There, the jet spreads only in the outward direction changing from the oval to the circular shape farther downstream. This mechanism seems to not be influenced by θ but rather by the aerodynamic effect of the flow through the nozzles with higher AR. The transition into the circular shape is much faster for SP jet than for the smooth transition ones (this does not translate into the faster spreading rates). The contours shape transition is substantially different for OP and SC nozzles. The arrows in Fig. 5c) and d) indicate the directions of this transition. It is evident that the profiles shrink along the major axis of the nozzle and at the same time expand towards the minor axis. Further downstream the initial triangular profiles are blurred however the orientation of the initial shape is inverted. This is an indication of the axis switching phenomena. Most likely due to the approximately uniform distribution of θ along the nozzle perimeter.

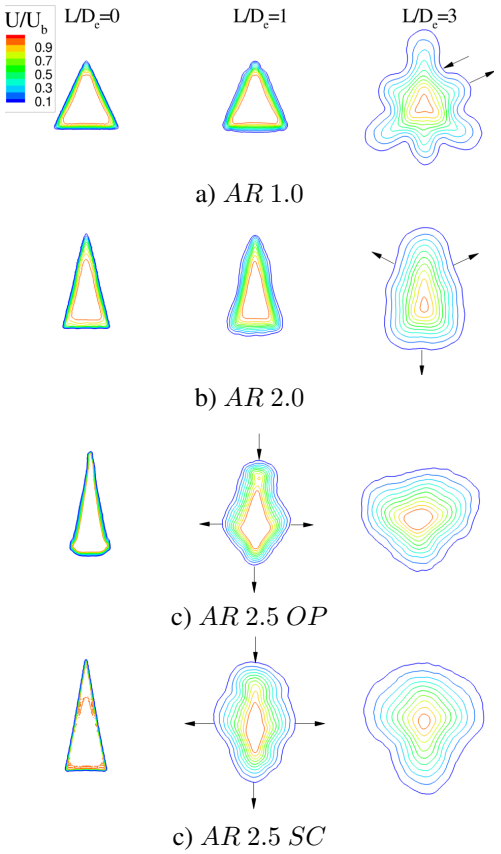

Figure 5: Contours of the averaged axial velocity on the planes perpendicular to the jet axis at three axial locations.

Finally, we want to take a closer look into the origin of the broad peak in U_{RMS}/U_c for AR 2.5 OP nozzle (Fig. 2d)). As suggested by Mi and Nathan (2010) this is the manifestation of the axis switching phenomena. We found however that even though the axis switching is observed also for SC nozzle the broad peak of U_{RMS}/U_c is not present in that case. This suggests that the broad peak have different origin than the axis-switching, likely due to the highly energetic turbulent structures merging in the jet centreline.

PSD and integral length scale

The power spectra (PSD) of the velocity fluctuations are shown in Fig. 6. For smooth transition nozzles we discerned two distinct peaks in the jet potential core region for all the AR cases. First one appearing approximately at $L_c/2$ and the second one further downstream at L_c, most likely stemming from the two phenomena, i.e., shear layer vortex shedding and vortex merging at the end of the potential core. The frequencies in terms of the Strouhal number (St) of those peaks for the AR 1.0 jet are $St \approx 0.68$ and 0.35, respectively. Increasing AR the frequencies of

the peaks slightly decrease. Differently from the

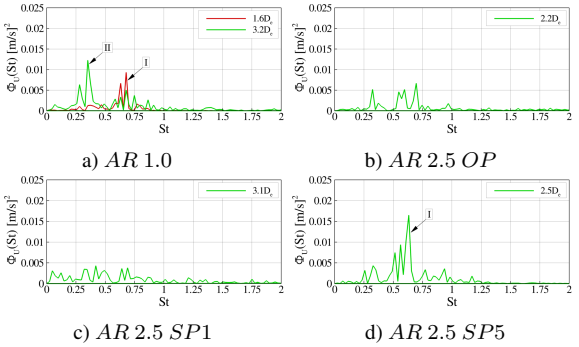

a) AR 1.0 b) AR 2.5 OP

c) AR 2.5 $SP1$ d) AR 2.5 $SP5$

Figure 6: Power spectral densities of the centreline signal of axial velocity fluctuations.

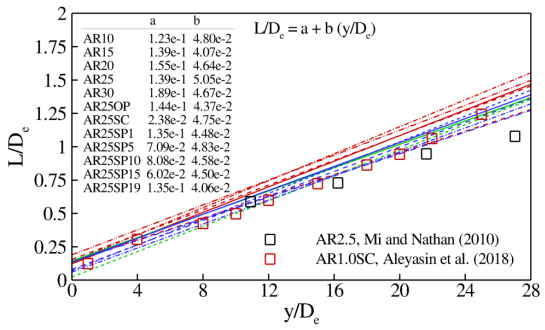

Figure 7: Centreline integral length scale evolution (linear fits). For lines legend see Fig. 2.

smooth transition nozzles, no evident peak but rather a broadband power distribution was found for OP, SC and AR 2.5 $SP1$ cases. This somewhat contradicts with findings of Quinn and Azad (2013) who found for AR 1.9 OP case the dominant peak at $St = 0.53$ (however for $Re = 168\,000$). Regarding the PSD in cases other than AR 2.5 $SP1$, a single peak in the range from $St = 0.6 \pm 0.1$ up to 0.7 occurs. However without a clear correlation to the location of the velocity signal extraction. It prevails at $L_c/D_e = 2.6 \pm 0.1$ for other cases and its power diminishes while progressing further downstream.

Finally, we analyse the centreline integral scale L/D_e evolutions calculated from the time signal autocorrelation function, following the expression:

$$L = U_b \int_{t_1}^{t_2} R_{uu} dt, \qquad (2)$$

in which we use U_b to estimate the length scale. The linear fits of the L/D_e evolution along the jets centrelines with fits functions are presented in Fig. 7. As can be seen, L increases linearly with the streamwise distance approaching $L/D_e = 1$ close to the $y/D_e \approx 20$, similarly as in Aleyasin et al. (2018).

4 Conclusions

The obtained results show that increasing the AR of a nozzle speeds-up the decay of the axial velocity and increases the growth of its fluctuations in the near-field. It is found that the impact of the AR on the jet behaviour strongly depends on the type of the exit nozzle section. A systematic parametric study allowed to univocally assess in which cases the alteration of AR causes qualitative or/and quantitative changes. Having a deep insight into the flow dynamics we were able to identify the mechanism (structures) causing the exceptional behaviour of the triangular jets.

Acknowledgments

This work is supported by National Science Center in Poland (Grant 2018/31/B/ST8/00762) and statutory funds of Department of Thermal Machinery (Czestochowa University of Technology) and the International Academic Partnerships Programme No. PPI/APM/2019/1/00062 sponsored by National Agency for Academic Exchange (NAWA).

References

Aleyasin, S.S, Fathi, N., Tachie, M.F., Vorobieff, P. and Koupriyanov, M. (2018), On the development of incompressible round and equilateral triangular jets due to Reynolds number variation, *J. Fluids Eng.*, Vol. 140, pp. 1-12.

Azad, M., Quinn, W. R. and Groulx, D. (2012), Mixing in turbulent free jets issuing from isosceles triangular orifices with different apex angles, *Exp. Th. Fluid Sci.*, Vol. 39, pp. 237–251.

Geurts, B.J. (2011), Direct and Large-Eddy Simulation, De Gruyter Series in Computational Science and Engineering

Gutmark, E.J. and Grinstein, F.F. (1999), Flow control with noncircular jets, *Annu. Rev. Fluid Mech.*, Vol. 31, pp. 239-272.

Mi, J., Nathan, G.J. and Luxton, R.E. (2000), Centreline mixing characteristics of jets from nine differently shaped nozzles, *Exp. Fluids*, Vol. 28, pp. 93-94.

Mi, J., Nathan, G.J. (2010), Statistical properties of turbulent free jets issuing from nine differently-shaped nozzles, *Flow, Turbul. Combust*, Vol. 84, pp. 583–606.

Schadow, K.C., Gutmark, E.J., Parr, D.M. and Wilson, K.J. (1988), Selective control of flow coherence in triangular jets, *Exp. Fluids*, Vol. 6, pp. 129-135.

Tyliszczak, A. (2014), A high-order compact difference algorithm for half-staggered grids for laminar and turbulent incompressible flows, *J. Comput. Phys.*, Vol. 276, pp. 438-467.

Quinn, W.R. (2005), Measurements in the near flow field of an isosceles triangular turbulent free jet, *Exp. Fluids*, Vol. 39, pp. 111–126.

Quinn, W.R., Azad, M. (2013), Mean streamwise centerline velocity decay and entrainment in triangular and circular jets, *AIAA Journal*, Vol. 51, pp. 70-79.